

Time scale of forerunners in quantum tunneling

G. García Calderón,^{1,*} Jorge Villavicencio,^{1,2,†} F. Delgado,^{3,‡} and J. G. Muga^{3,§}

¹*Instituto de Física, Universidad Nacional Autónoma de México
Apartado Postal 20 364, 01000 México, D.F., México*

²*Facultad de Ciencias, Universidad Autónoma de Baja California
Apartado Postal 1880, 22800 Ensenada, Baja California, México*

³*Departamento de Química-Física, UPV-EHU,
Apartado 644, 48080 Bilbao, Spain*

The forerunners preceding the main tunneling signal of the wave created by a source with a sharp onset or by a quantum shutter, have been generally associated with over-the-barrier (non-tunneling) components. We demonstrate that, while this association is true for distances which are larger than the penetration length, for smaller distances the forerunner is dominated by under-the-barrier components. We find that its characteristic arrival time is inversely proportional to the difference between the barrier energy and the incidence energy, a tunneling time scale different from both the phase time and the Büttiker-Landauer (BL) time.

PACS numbers: 03.65.Xp, 03.65.Ta, 03.65.-w

I. INTRODUCTION

Tunneling is one of the paradigms of quantum theory. Textbooks only discuss its stationary aspects, emphasizing the non-vanishing transmission probability for monochromatic wavefunctions with energies below the barrier maximum. In recent times, since the seminal work of Büttiker and Landauer [1], its time dependent aspects have been also investigated to find characteristic time scales that summarize, together with the transmittance, the system behavior. Much of this work has been controversial, as several authors have proposed and defended different “tunneling times”. In fact each has its own virtues, weaknesses, and range of applicability. For a recent and rather extensive multi-author review see [2]; for previous reviews see [3, 4, 5, 6]. An analysis of the involved non-commuting observables (the projectors that determine the final transmission and the probability to find the particle in the barrier region) shows that, from a fundamental perspective, there is no unique tunneling time, because several quantizations are possible due to different operator orderings and defining criteria [7].

This does not mean though that the timing question should be abandoned. Rather, it is necessary to specify more precisely how to time the quantum particle in the tunneling regime. Different specifications lead to different relevant time scales; in other words, the importance of the differently defined times rests on the context where they become physically significant quantities. For example, the traversal time of Büttiker and Landauer (BL time)[1], $\tau = L/v_{sc}$, given by the barrier length L divided by the “semiclassical” velocity $v_{sc} = [2(V - E)/m]^{1/2}$,

marks the transition from sudden to adiabatic regimes for an oscillating barrier [1], and determines the rotation of the spin in a weak magnetic field in opaque conditions [8]; whereas the average over wavepacket components of the (monochromatic) “phase times” provides the mean arrival time of the transmitted wave packet [7, 9]. These two time scales may be very different. The Büttiker-Landauer time increases with decreasing energies up to a finite value, whereas $\tau^{Ph}(0, L)$ (the so called extrapolated phase time) diverges as $E \rightarrow 0$, and tends for increasing L to a constant value, $2\hbar/[v_{sc}(2mE)^{1/2}]$. This later property implies that the arrival of the transmitted wave becomes independent of L (Hartman effect [10]), although the independence only holds until a certain critical length L_c [7] where above-the-barrier components start to dominate. For $L > L_c$ the mean arrival time depends on L linearly. While τ and τ^{Ph} are surely the most frequently invoked tunneling times, they do not exhaust all timing questions.

In particular, in Ref. [11], the time $t_{tr} = t_{tr}(x)$ that characterizes the transition from the transient to the stationary regime for a wave formed by a point source with a sharp onset, was identified and the time of arrival, $t_p = t_p(x)$, of the peak of the forerunner at a point x in opaque conditions was also identified. Here “opaque” means $x\kappa_0 \gg 1$, where $\kappa_0 = [2m(V - E_0)]^{1/2}/\hbar$, and $E_0 = \hbar\omega_0$. This particular time scale turned out to be (surprisingly) proportional to the BL time τ *i.e.*,

$$t_p = \tau/3^{1/2}, \quad (1)$$

even though the time-frequency analysis of the forerunner showed that it was composed by frequencies above threshold. In other words, it corresponded to non-tunneling. In spite of its frequency content, the forerunner’s peak “travels” with a velocity proportional to v_{sc} , $v_p = 3^{1/2}v_{sc}$, which increases with decreasing energies, and its intensity diminishes exponentially as it progresses along the coordinate x . Other works had already pointed out the dominance of non-tunneling components

*Electronic address: gaston@fisica.unam.mx

†Electronic address: villavics@uabc.mx

‡Electronic address: qfbdeacf@lg.ehu.es

§Electronic address: qfpmufrj@lg.ehu.es

in the forerunner [12, 13, 14, 15, 16] but had not characterized its time dependence. Their main objective was to show that a previous prediction by Stevens [17] (who believed that a tunneling monochromatic ω_0 -front, associated with a pole at ω_0 in the complex frequency plane would arrive at τ) did not hold because of the effect of the saddle point or other critical points, such as resonances in a square barrier model [16]. (For the source-with-a-sharp-onset model the frequency of the saddle is given by $\omega_s = E_s/\hbar$, where the saddle energy, $E_s = V + x^2m/2t^2$, coincides with the energy of a classical particle traveling from the source to x in a time t .) Büttiker and Thomas [18] proposed to enhance the importance of the monochromatic front associated with ω_0 compared to the forerunners by limiting the frequency band of the source or of the detector; it was shown later in [11] that the monochromatic front could not be seen in opaque conditions even with the frequency band limitation. However, a clear separation of the amplitude into two terms, one associated with saddle and forerunner and the other with the pole and the “monochromatic front”, is only possible for opaque conditions. Non semiclassical conditions have been much less investigated [19], even though these are actually easier to observe because of the stronger signal. In this paper we shall be mainly concerned with them.

The motivation of the present paper is a recent publication of two of us where the time evolution of an initial cutoff wave truncated at the left edge of a square barrier (shutter problem) [20] was examined. There it was found that the probability density at the barrier edge $x = L$, exhibits at short times a transient structure named *time domain resonance*. The maximum, t_p , of the *time domain resonance* showed a plateau region for small L , or more accurately a shallow basin, followed by a linear dependence for larger L ; this behavior is reminiscent of the Hartman effect, but the time of the plateau did not coincide with the phase-time estimate. It was found that for a broad range of parameters, t_p in the basin may be written approximately as,

$$t_p^B = \frac{\hbar\pi}{\epsilon_1 - E_0}, \quad (2)$$

where ϵ_1 and E_0 , correspond to the energy of the first top-barrier resonance and the incidence energy, respectively. Such a dependence had not been described before. On the other hand, along the linear regime, at larger values of L , t_p is described by,

$$t_p^L = \frac{L}{v_1}, \quad (3)$$

where $v_1 = \hbar a_1/m$, with a_1 the real part of the first top-barrier pole $k_1 = a_1 - ib_1$. The above time scales are also different from the BL-time, even though they may coincide with t_p^L for a particular value of L .

We shall show in this paper that this basin dependence, and the corresponding time scale, is not only present at the transmission edge of the square barrier studied in [20].

It may also be found, *mutatis mutandis*, in the sharp onset source model examined in [11] for small $x\kappa_0$. We also find the basin for the time of the forerunner versus position in the internal region of the square barrier, and for a step potential barrier. There are not resonances in the sharp onset source model, or for the step potential, so the time scale of the basin minimum is in these cases inversely proportional to κ_0^2 , namely to the difference between the “potential level” V and the source main energy E_0 . This is to be contrasted with the dependence on κ_0^{-1} of the traversal time τ .

An important open question was to determine if the forerunner at small lengths in the evanescent region corresponds or not to tunneling frequencies. We shall show by a simple time-frequency analysis that the peak of the forerunner in this regime is composed predominantly by under-the-barrier components, so that indeed a genuine tunneling time scale different from phase or BL times has been found.

In section II the source with a sharp onset is discussed, and in section III we shall examine the internal region of the square barrier, as well as the step barrier case. As the reader will soon discover, apart from certain peculiarities, all models show a small length region of the order of the penetration length κ_0^{-1} where the forerunner is dominated by tunneling components and arrives at a time proportional to κ_0^{-2} .

II. SOURCE WITH A SHARP ONSET

A. Formalism

The time dependent solution of the Schrödinger equation for a potential $V(x) = V$ that occupies the entire space, subject to a source boundary condition,

$$\psi(0, t) = e^{-i\omega_0 t/\hbar} \Theta(t), \quad (4)$$

has the form, [11]

$$\Psi(x, t) = \frac{1}{2} e^{-itV/\hbar + ix^2/(4C^2t)} [w(-u'_0) + w(-u''_0)], \quad (5)$$

where $w(z) = e^{-z^2} \operatorname{erfc}(-iz)$ and

$$u'_0 = \frac{1+i}{2^{1/2}} t^{1/2} C\kappa_0 \left(-i - \frac{\tau}{t}\right), \quad (6)$$

$$u''_0 = \frac{1+i}{2^{1/2}} t^{1/2} C\kappa_0 \left(i - \frac{\tau}{t}\right), \quad (7)$$

$$\tau = x/v_{sc} = xm/\kappa_0\hbar, \quad (8)$$

$$C = (\hbar/2m)^{1/2}. \quad (9)$$

In the opaque limit ($x\kappa_0 \gg 1$), an excellent approximation is given by adding up the pole and saddle terms,

$$\Psi(x, t) \approx \Psi_0 + \Psi_s, \quad (9)$$

$$\Psi_0 = e^{-i\omega_0 t} e^{-\kappa_0 x} \Theta(t - \tau), \quad (10)$$

$$\Psi_s = \frac{1}{2i\pi^{1/2}} e^{-\frac{itV}{\hbar} + \frac{ix^2}{4C^2t}} \left(\frac{1}{u'_0} + \frac{1}{u''_0} \right). \quad (11)$$

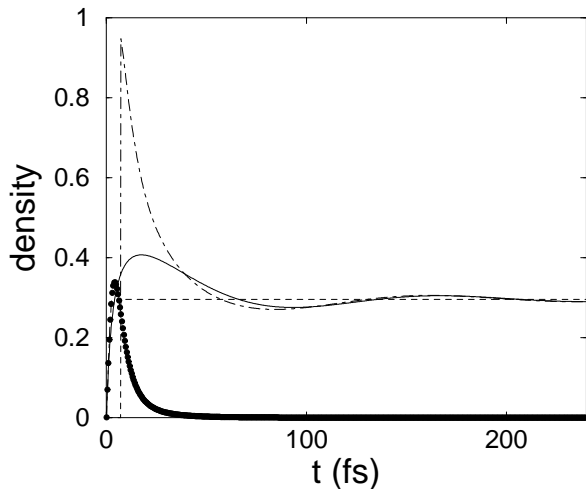


FIG. 1: $|\Psi|^2$ (solid line), $|\Psi_s|^2$ (circles), $|\Psi_0|^2$ (dashed line), and $|\Psi_0 + \Psi_s|^2$ (dotted-dashed line) versus t for $E_0 = 0.907V$, and $x = 2.75$ nm. Here and in Figs. 2-6, $V = 0.3$ eV. In all figures $m = 0.067m_e$, where m_e is the electron's mass.

For opaque conditions at fixed x the saddle term is totally dominant in the forerunner peak; at later times it fades away and the pole (tunneling) term becomes dominant. This allowed to identify t_p from the peak of $|\Psi_s|^2$, and t_{tr} as the time where the two contributions were of equal importance. The small $x\kappa_0$ regime did not permit the same approximation treatment, so that t_p could not be characterized by the formula found for the opaque case, Eq. (1). It may be argued however, that the small $x\kappa_0$ case is in fact more interesting since it allows non-negligible signals (densities), whereas for large opacity the signal becomes exponentially small and very hard to detect.

B. Examples

In Fig. 1 we have depicted the density versus t for a fixed x smaller than the penetration length $1/\kappa_0$ for the source-with-a-sharp-onset model. In all calculations the effective mass of the electron is taken as $m = 0.067m_e$. The forerunner is identified as a smooth broad bump with its peak at t_p . The contributions of the saddle and pole terms are also drawn, as well as the contribution of their sum. The saddle term reproduces the density only for very short times while the pole gives the large time behavior.

In Fig. 2 the average local frequency [11, 21], $\omega_{av} = -\text{Im}[(d\Psi/dt)/\Psi]$, the frequency of the saddle ω_s , and ω_0 are shown, relative to ω_V , versus t for the same value of x . Note that ω_{av} tends to ω_0 for large t , and to ω_s for very short times, going from ω_s to ω_0 during the time span of the forerunner bump (compare with the density in Fig. 1); in particular $\omega_{av}/\omega_V < 1$ at the peak t_p . Fig. 3 shows the dependence with x of the time of arrival of the peak of the forerunner, t_p , for two differ-

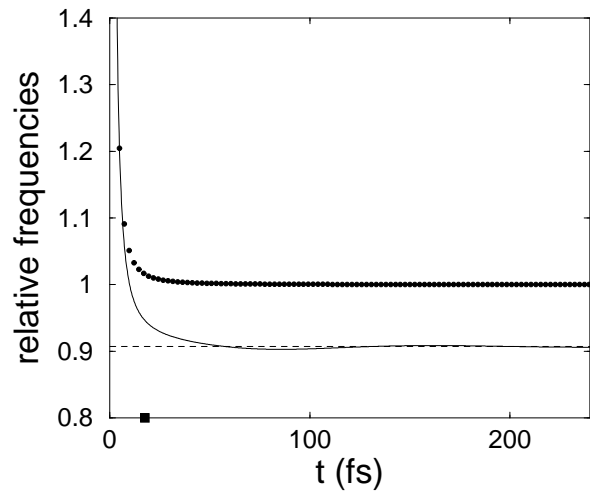


FIG. 2: ω_{av}/ω_V (solid line), ω_0/ω_V (dashed line), and ω_s/ω_V (circles) versus t for the same parameters of Fig. 1. The square marks the value of t_p .

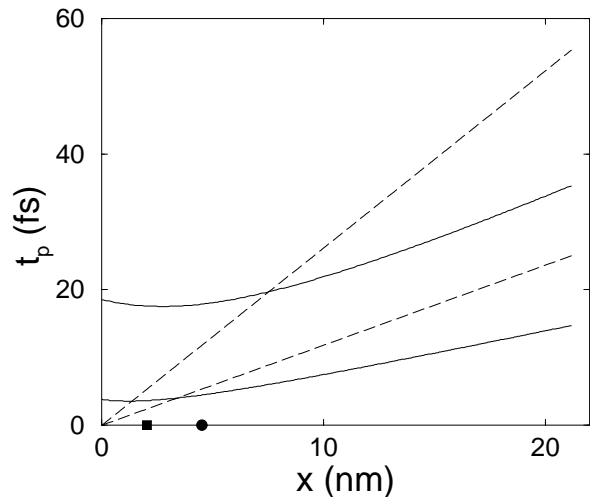


FIG. 3: time of arrival of the forerunner's peak versus x for $\omega_0 = 0.907\omega_V$ (upper solid line), and $\omega_0 = 0.544\omega_V$ (lower solid line). The upper and lower dashed lines are the corresponding BL-times. The values of $1/\kappa_0$ are also shown with a square ($\omega_0 = 0.544\omega_V$) and a circle ($\omega_0 = 0.907\omega_V$)

ent values of ω_0 . The (unsharp) transition between the quasi-plateau region at lower x and the linear regime for larger x occurs around a few penetration lengths $1/\kappa_0$. Thus, a smaller ω_0 implies a more reduced plateau. Also shown are the corresponding Büttiker-Landauer times for comparison. In the plateau region the forerunner's peak does not travel but arrives roughly simultaneously at all x (in fact up to the basin minimum the forerunner arrives earlier at larger x !); beyond the plateau region the forerunner, whose peak is characterized in that case by Eq. (1), arrives later at larger x , and becomes dominated by frequencies “above the barrier”.

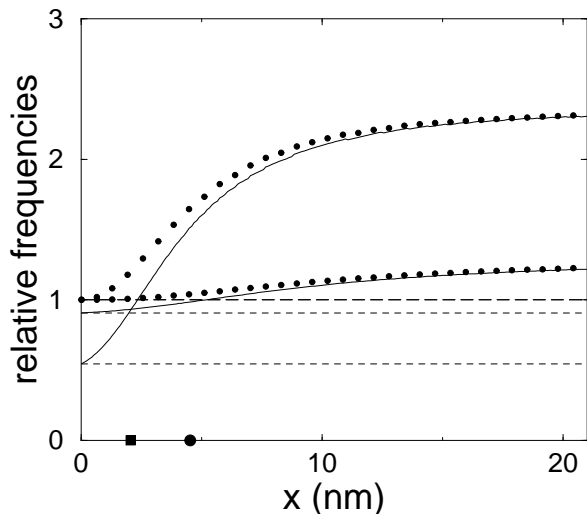


FIG. 4: ω_{av}/ω_V (solid line), ω_0/ω_V (short dashed line), and ω_s/ω_V (circles) for the same cases of Fig. 3. Upper curves: $\omega_0 = 0.907\omega_V$; lower curves: $\omega_0 = 0.544\omega_V$. The values of κ_0^{-1} are indicated as in Fig. 3

Fig. 4 shows the average frequency ω_{av} calculated right at the forerunner's peak at the time $t_p(x)$ for each value of x , as well as ω_s , and ω_0 , all relative to ω_V , for the same two values of ω_0 of the previous figure. The forerunner's peak frequency begins at ω_0 at $x \rightarrow 0$, then it grows smoothly and becomes non-tunneling (ω_{av}/ω_V crosses 1) around $1/\kappa_0$. For larger x , ω_{av} tends to the saddle frequency ω_s . Further insight into the nature of the tunneling forerunner is obtained by looking at a series of snapshots of the wave density versus x (instead of looking at density versus time for a fixed location). The plateau, or rather shallow basin, must be, according to Fig. (3), the result of a "breathing" transient mode of the evanescent wave, which implies an essentially simultaneous growth of the wave for all x up to a few penetration lengths, and until the maximum is achieved at t_p . This is indeed confirmed in Fig 5, where several snapshots of the density are taken at five different times. In the final one the wave is already close to its asymptotic (large time) form. The linear dependence of the time of arrival of the peak with κ_0^{-2} is shown in Fig. 6, which is drawn by choosing the values of $V - E_0$ and t_p corresponding to the minima of the shallow basins obtained for different values of E_0 (see Fig. 3).

III. QUANTUM SHUTTER

A. Formalism

Assume now an arbitrary potential $V(x)$ ($0 \leq x \leq L$) that vanishes outside the internal region, and the initial

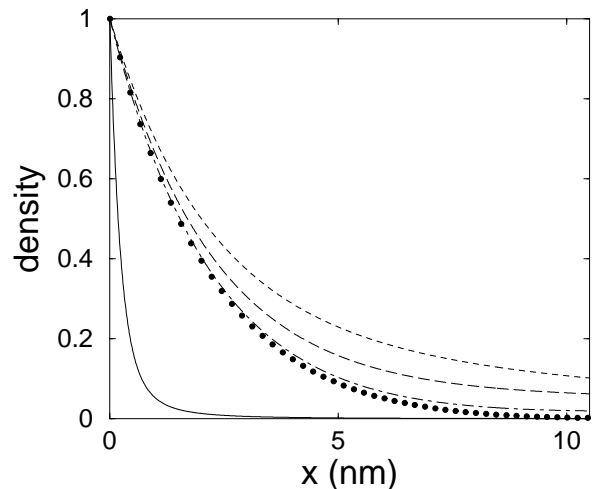


FIG. 5: Density $|\Psi|^2$ versus x for $\omega_0/\omega_V = 0.907$ and $t = 0.05, 24, 48, 72$ and 97 ns (solid, short-dashed, long-dashed, dot-dashed, and circles respectively).

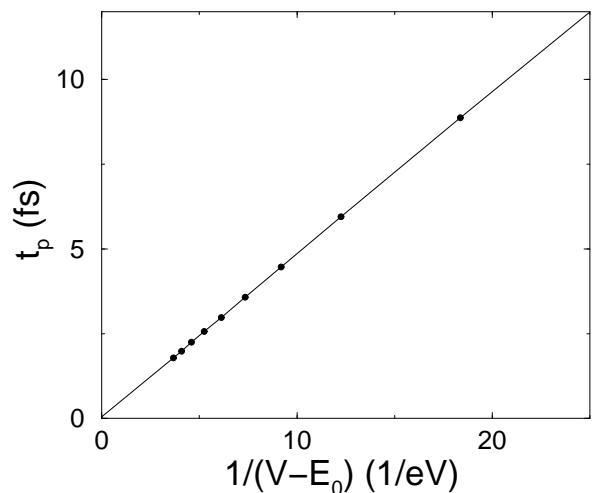


FIG. 6: Time of arrival of the forerunner's peak t_p versus $1/(V - E_0)$ at the position that minimizes t_p for a given E_0 , see Fig. 3. As in all the figures of this section, $V = 0.3$ eV.

condition,

$$\Psi(x, k; t = 0) = \begin{cases} e^{ikx} - e^{-ikx}, & -\infty < x \leq 0, \\ 0, & x > 0, \end{cases} \quad (12)$$

which corresponds to a plane wave impinging on a perfectly reflecting shutter placed at $x = 0$, just at the left edge of the structure. The time dependent process begins with the instantaneous opening of the shutter at $t = 0$, enabling the incoming wave to interact with the potential at $t > 0$. The exact solution along the internal region ($0 \leq x \leq L$) is given by [22],

$$\Psi^i = \phi_k M(y_k) - \phi_{-k} M(y_{-k}) - \sum_{n=-\infty}^{\infty} \rho_n M(y_{k_n}). \quad (13)$$

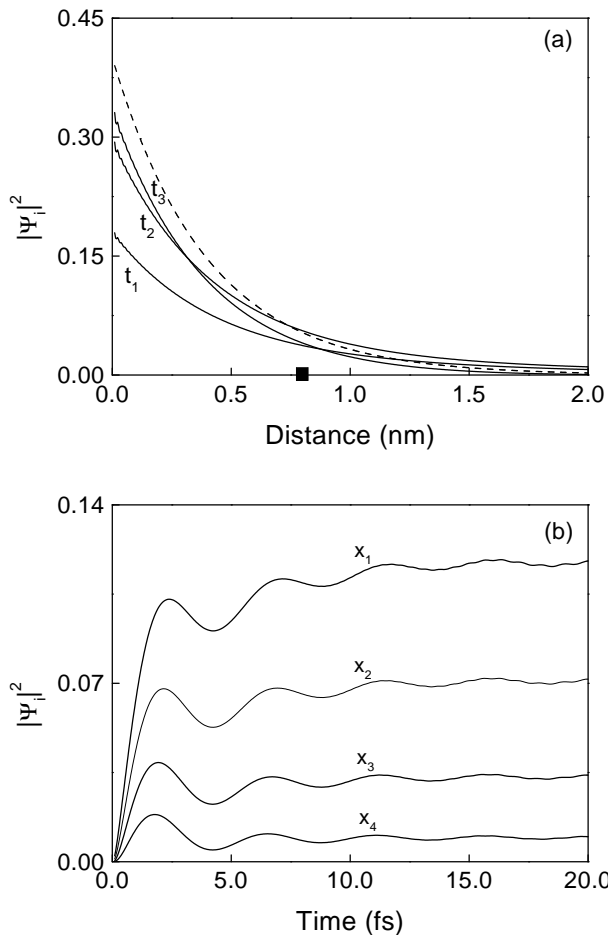


FIG. 7: (a) Snapshots of $|\Psi^i|^2$ (solid line) taken at different values of time: $t_1 = 1.0$ fs, $t_2 = 2.0$, and $t_3 = 4.0$ fs. The stationary solution $|\phi_k|^2$ is included for comparison, and a full square indicates the value of κ_0^{-1} , which is the penetration length of the stationary solution. (b) Time evolution of $|\Psi^i|^2$ at different fixed values of the position x : $x_1 = 0.5$ nm, $x_2 = 0.7$ nm, $x_3 = 1.0$ nm, and $x_4 = 2.0$ nm. The solution exhibits a behavior similar to diffraction in time pattern.

In the above expressions, the quantities $\phi_{\pm k}$ refer to the stationary solution, and the factor $\rho_n = 2iku_n(0)u_n(x)/(k^2 - k_n^2)$ is given in terms of the resonant eigenfunctions, $\{u_n(x)\}$, with complex eigenvalues [22] $k_n = a_n - ib_n$ ($a_n, b_n > 0$). The index n runs over the complex poles k_n , distributed in the third and fourth quadrants in the complex k -plane. Both the complex poles $\{k_n\}$ and the corresponding resonant eigenfunctions $\{u_n(x)\}$, can be calculated using a well established method, as discussed elsewhere [20, 22]. In the above equation the M functions are defined as,

$$M(y_q) = \frac{1}{2}w(iy_q), \quad (14)$$

where $y_q = -e^{-i\pi/4}[(\hbar/2m)t]^{1/2}q$, $q = \pm k$, and $k_{\pm n}$.

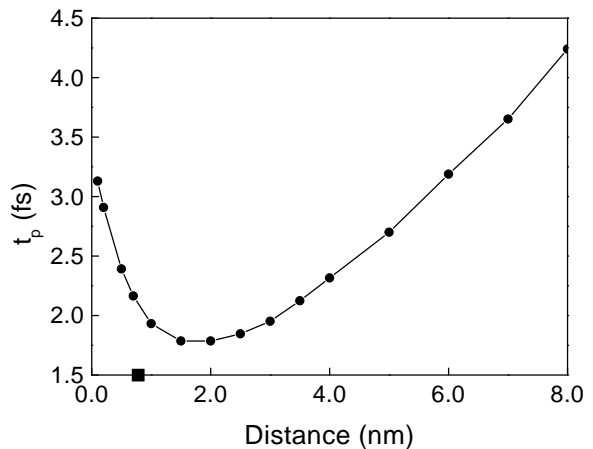


FIG. 8: Exact calculation of t_p (solid dots) as a function of the position x . The parameters are the same as in Fig. 7. A full square indicates the value of κ_0^{-1} .

B. Examples

In what follows we shall explore the features of the probability density along the internal region of one-dimensional rectangular potential barriers of height V and thickness L , defined along the interval $0 \leq x \leq L$. We choose the following parameters: $V = 1.0$ eV, $L = 40.0$ nm, and incidence energy $E_0 = \hbar^2 k^2 / 2m = 0.1$ eV. For this particular case the full barrier is opaque, $\alpha \equiv L[2mV]^{1/2} / \hbar = 53.0$, but we are interested in distances of the order of, or smaller than, the penetration length $\kappa_0^{-1} \ll L$. In Fig. 7 (a) we use Eq. (13) to explore the birth of the probability density along the internal region of the potential. Here we plot $|\Psi^i|^2$ (solid line) as a function of small values of the position x , for increasing values of time. Notice that as time increases, the probability density evanesces along the internal region swinging around the stationary solution (dashed line).

In Fig. 7 (b) we illustrate the time dependence of the transient “swinging mode” exhibited in Fig. 7 (a). We exhibit the behavior of $|\Psi^i|^2$ (solid line) as a function of time for several values of the position x_i ($i = 1, 2, 3, 4$). The probability density grows monotonically until it reaches its first maximum value, and oscillates thereafter as it tends to the stationary situation given by $|\phi_k|^2$ [22]. Here we observe again a peculiar behavior in the time evolution of $|\Psi^i|^2$, presented in plot (b) of Fig. 7: the first maximum of the probability density appears earlier at larger values of x . In Fig. 8 we plot the exact calculation of t_p (solid dots), which corresponds to the peak value of the first maximum of $|\Psi^i|^2$, measured at different values of the position, x .

In Fig. 8 we can clearly identify two regimes, as in the case of Fig. 3. The first of them corresponds to a basin, where for small values of the position, t_p decreases reaching a minimum value as x increases. This is in ac-

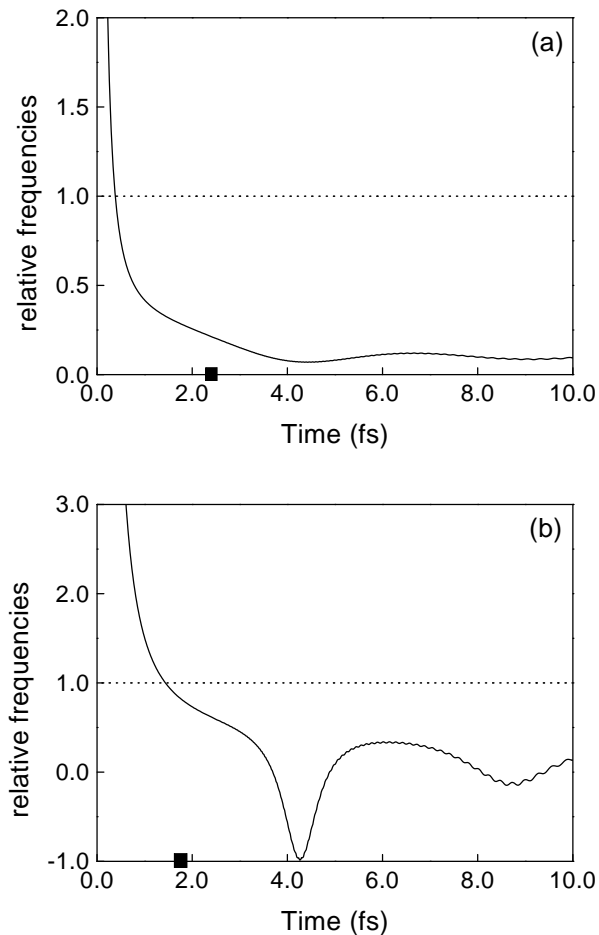


FIG. 9: Plot of the relative local frequency ω_{av}/ω_V (solid line) for the positions (a) $x_1 = 0.5$ nm, and (b) $x_4 = 2.0$ nm, corresponding to the cases depicted in Fig. 7 (b). The cutoff-frequency $\omega_V/\omega_V = 1$ (dotted line) is included for comparison, and a full square indicates the position of t_p .

cordance with the observed behavior of the maximum in Fig. 7 (b). However, if x is further increased, t_p begins to grow as a function of the position. Apparently this second regime corresponds to a situation where t_p increases linearly with x . The result depicted in Fig. 8 appears to be a replica of a similar behavior of the probability density at the barrier edge $x = L$, recently reported in Ref. [20].

We have also analyzed the frequency content of $|\Psi^i|^2$ along the internal region. In Fig. 9 (b) we plot ω_{av}/ω_V along the relevant time interval for some of the values of the position, depicted in Fig. 7 (b). We can appreciate that the probability density at this small values of the position x , is composed entirely by under-the-barrier frequency components i.e $\omega_{av}/\omega_V < 1$ in the vicinity of the maximum t_p . Notice that this result is similar to the one obtained in Fig. 2.

Finally, Fig. 10 shows the linear dependence of the time corresponding to the basin minimum with respect to

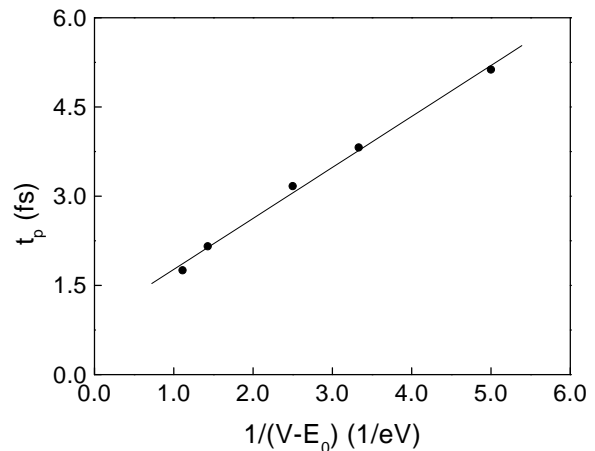


FIG. 10: Maximum of the *time domain resonance*, t_p , as a function of $1/(V - E_0)$. The parameters are the $V = 1.0$ eV, and $L = 40.0$ nm.

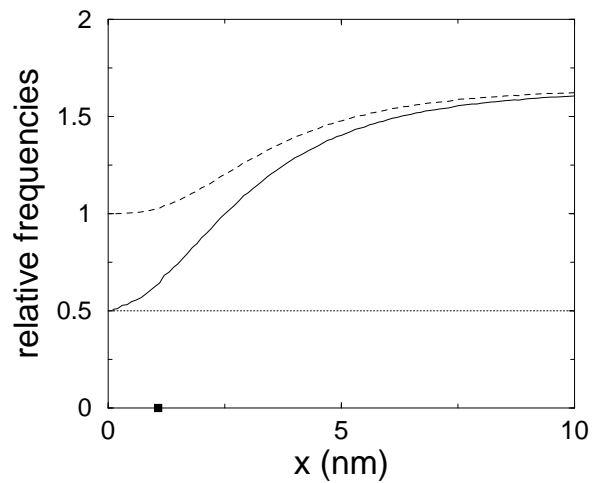


FIG. 11: ω_{av}/ω_V (solid line), ω_0/ω_V (dotted line), and ω_s/ω_V (dashed line) for $V = 1$ eV and $E_0 = 0.5$ eV. The value of κ_0^{-1} is indicated with a square.

$1/(V - E_0)$ in analogy to the analysis of the point source problem. Note, however, that in our case we could also have considered a plot with respect to $1/(\varepsilon_1 - E_0)$ with a similar result since it turns out that for opaque barriers $\varepsilon_1 \approx V$.

C. Potential step

The potential step $V\Theta(x)$ requires a different formal treatment [23] but very similar results are found. We have evaluated $\langle x|\Psi(t)\rangle$ by means of an integral over the energy eigenfunctions for the the initial state,

$$\Psi(x, k; t = 0) = \begin{cases} e^{ikx}, & -\infty < x \leq 0, \\ 0, & x > 0. \end{cases} \quad (15)$$

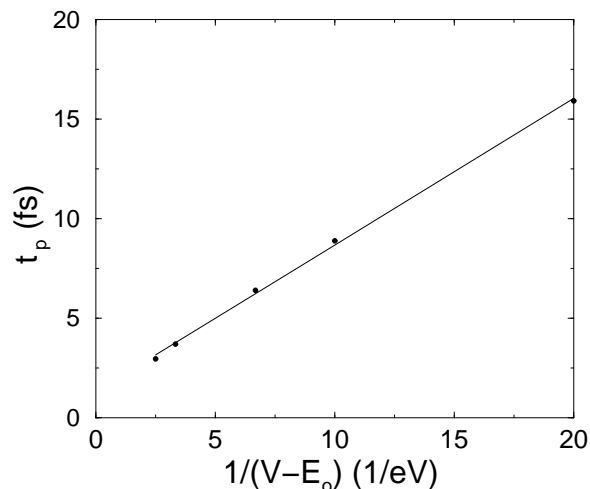


FIG. 12: Time of arrival of the forerunner's peak t_p versus $1/(V - E_0)$ at the position that minimizes t_p for a given E_0 . $V = 1$ eV.

In Fig. 11 the average frequency peak of the forerunner is shown versus x for this system. As in the source with a sharp onset case, it goes from ω_0 to ω_s , crossing the threshold frequency at approximately $2/\kappa_0$. Fig. 12 shows also the linear dependence of the time of the forerunner (calculated at its minimum value for a given energy, *i.e.*, at the basin minimum) versus $1/(V - E_0)$.

IV. FINAL COMMENTS

By using different time-dependent models of quantum waves impinging on a potential barrier, we have shown

the existence of forerunners dominated by under-the-barrier components. These transient structures are indeed associated with a true tunneling process, occurring at distances smaller than the penetration length, κ_0^{-1} . We find that the time of arrival is proportional to $1/(V - E_0)$, where E_0 stands for the incidence energy, chosen below the barrier height, V . This is in contrast to the dominance of above the barrier frequencies for larger distances, and to other well known tunneling time scales such as the Büttiker-Landauer or "phase" times.

These results suggest a number of questions that need further investigation. For example, the proportionality constant observed in the arrival times of the forerunner's peak, depends on the peculiarities of each model, and a general theory for its specific value should be found. Also, the Larmor time for spin rotation defined by Büttiker is given for very thin barriers by \hbar/V in the limit $k = 0$ [8]. In spite of the very different ways in which the Larmor time and the forerunner's peak time are obtained, these two quantities might be related. Finally, we hope that the results presented may motivate an experimental search of tunneling forerunners and their corresponding time scale.

Acknowledgments

We are grateful to M. Büttiker for commenting on a preliminary version of the manuscript. JGM and FD acknowledge support by Ministerio de Ciencia y Tecnología (BFM2000-0816-C03-03), UPV-EHU (00039.310-13507/2001), and the Basque Government (PI-1999-28). GC and JV acknowledge financial support from Conacyt, México, through Contract No. 431100-5-32082E, and GC that of DGAPA-UNAM under grant IN101301.

-
- [1] M. Büttiker and R. Landauer, Phys. Rev. Lett. **49**, 1739 (1982).
 - [2] *Time in Quantum mechanics*, J. G. Muga, R. Sala, I. L. Egusquiza (eds.) (Springer-Verlag, Berlin, 2002).
 - [3] E.H. Hauge, J.A. Stovngeng, Rev. Mod. Phys. **61**, 917 (1989).
 - [4] C.R. Leavens, G.C. Aers: in *Scanning Tunneling Microscopy and Related Techniques*, ed. by R. J. Behm, N. García, H. Rohrer (Kluwer, Dordrecht, 1990)
 - [5] R. Landauer and Th. Martin, Rev. Mod. Phys. **66**, 217 (1994)
 - [6] P. Ghose, *Testing Quantum Mechanics on New Ground* (Cambridge University Press, Cambridge, 1999), Chapter 10.
 - [7] S. Brouard, R. Sala and J. G. Muga, Phys. Rev. A **49**, 4312 (1994).
 - [8] M. Büttiker, Phys. Rev. B. **27**, 6178 (1983).
 - [9] J. G. Muga and C. R. Leavens, Phys. Rep. **338**, 353 (2000).
 - [10] T. E. Hartman, J. Appl. Phys. **33**, 3427 (1962).
 - [11] J. G. Muga and M. Büttiker, Phys. Rev. A **62**, 023808 (2000).
 - [12] A. Ranfagni, D. Mugnai, P. Fabeni and P. Pazzi, Physica Scripta **42**, 508 (1990).
 - [13] A. Ranfagni, D. Mugnai and A. Agresti, Phys. Lett. A **158**, 161 (1991).
 - [14] N. Teranishi, A. M. Krivan and D. K. Ferry, Superlattices and Microstructures, **3**, 509 (1987).
 - [15] A. P. Jauho and M. Jonson, Superlattices and Microstructures **6**, 303 (1989).
 - [16] S. Brouard and J. G. Muga, Phys. Rev. A **54**, 3055 (1996).
 - [17] K. W. H. Stevens, Eur. J. Phys. **1**, 98 (1980); J. Phys. C: Solid State Phys. **16**, 3649 (1983).
 - [18] M. Büttiker and H. Thomas, Ann. Phys. (Leipzig) **7**, 602 (1998); Superlattices Microstruct. **23**, 781 (1998).
 - [19] G. Nimtz, A. Haibel, and R. M. Vetter, in *Time's arrows, quantum measurement and superluminal behaviour*, (C.N.R., Roma, 2001) p. 125.
 - [20] G. García-Calderón and J. Villavicencio, Phys. Rev. A **64** 012107 (2001).
 - [21] L. Cohen, *Time-Frequency analysis* (Prentice Hall, New

- Jersey, 1995).
- [22] G. García-Calderón and A. Rubio, Phys. Rev. A **55**, 3361 (1997).
- [23] F. Delgado and J. G. Muga, unpublished results.